Two-dimensional wetting: The role of atomic steps on the nucleation of thin water films on BaF2(111) at ambient conditions

M. Cardellach, A. Verdaguer, J. Santiso, and J. Fraxedas

Citation: J. Chem. Phys. **132**, 234708 (2010); doi: 10.1063/1.3456698
View online: http://dx.doi.org/10.1063/1.3456698
View Table of Contents: http://jcp.aip.org/resource/1/JCPSA6/v132/i23
Published by the American Institute of Physics.

Two-dimensional wetting: The role of atomic steps on the nucleation of thin water films on $BaF_2(111)$ at ambient conditions

M. Cardellach, A. Verdaguer,[a] J. Santiso, and J. Fraxedas
Centre d' Investigació en Nanociència i Nanotecnologia, CIN2 (CSIC-ICN), Esfera UAB, Campus de la UAB, Edifici CM-7, Bellaterra, Catalunya 08193, Spain

(Received 11 March 2010; accepted 3 June 2010; published online 21 June 2010)

The interaction of water with freshly cleaved $BaF_2(111)$ surfaces at ambient conditions (room temperature and under controlled humidity) has been studied using scanning force microscopy in different operation modes. The images strongly suggest a high surface diffusion of water molecules on the surface indicated by the accumulation of water at step edges forming two-dimensional bilayered structures. Steps running along the $\langle \bar{1}10 \rangle$ crystallographic directions show a high degree of hydrophilicity, as evidenced by small step-film contact angles, while steps running along other directions exhibiting a higher degree of kinks surprisingly behave in a quite opposite way. Our results prove that morphological defects such as steps can be crucial in improving two-dimensional monolayer wetting and stabilization of multilayer grown on surfaces that show good lattice mismatch with hexagonal ice. © *2010 American Institute of Physics*. [doi:10.1063/1.3456698]

I. INTRODUCTION

In spite of the fact that only a small percentage of the total condensed water in the troposphere is in the form of ice, this condensed form of water exerts a critical influence on important meteorological processes such as precipitation and cloud electrification.[1,2] The formation of ice in the troposphere at temperatures above −33 °C is induced mainly by a foreign body, the so-called ice nucleation agent or sublimation nuclei, in a process known as heterogeneous nucleation. The physicochemical properties and mechanisms involved in efficient heterogeneous nucleating surfaces are still not well understood[3] and this fact motivated many fundamental studies on the determination of the structure of water films adsorbed on surfaces at different length scales.[4]

There has been particular interest in the study of surfaces exhibiting hexagonal structure with surface lattice constants close to that of the basal plane of hexagonal (I_h) ice, the form of all natural snow and ice on Earth, because it was predicted that nearly lattice matching may readily induce nucleation of ice in ambient conditions triggering condensation of water from clouds.[5] The mostly studied compound has been AgI, although its efficiency in manmade cloud seeding has not been clearly demonstrated.[6] Heterogeneous nucleation is affected by other factors such as the presence of defects on the surface, the chemical nature of the surface and the chemical bonding with the adsorbing water molecules.[7] The relative importance of the mentioned factors on heterogeneous ice nucleation is still a matter of debate and to date predictions on the nature and structure of efficient ice nucleating materials are far from being reliable, although an attempt to correlate water structuring with the dipolar distribution at the surface has been recently introduced.[8]

The cleaved (111) face of the alkaliearth fluoride BaF_2 has been proposed as an ice nucleation agent since it exhibits a surface lattice constant (4.38 Å) close to that of I_h ice (4.52 Å).[9–14] The $BaF_2(111)$ surface consists of an hexagonal array of barium and fluoride ions, distributed in trilayers (F–Ba–F). Early experiments and simulations suggested that water adsorbed on $BaF_2(111)$ at ambient conditions would build I_h bilayer patches on the surface.[15] However, $BaF_2(111)$ turns out to be an inefficient nucleation agent and the growth of ice films on this surface was found to be unstable even at temperatures well below the freezing point.[16] Recent scanning probe microscopy (SPM) results have shown that, although water molecules form two-dimensional (2D) patches on this surface exhibiting a preferential mean dipolar orientation, the actual structure of water films on $BaF_2(111)$ can hardly correspond to an I_h ice bilayer.[14] In the same line, based on *ab initio* and density functional theory calculations, it was found that a single water molecule would adsorb preferentially with the oxygen on the barium ion and with the hydrogen atoms toward the neighboring fluorine ions.[12,17] Such molecular distribution would hinder the formation of a stable ice bilayer and thus of multilayers of I_h ice.

Another material exhibiting good lattice matching to hexagonal ice is kaolinite, a clay mineral with a quasihexagonal arrangement of hydroxyl groups. Simulations of water on the hydroxylated (001) surface of kaolinite revealed that, although a 2D icelike bilayer is stable, the orientation of the water molecules of this layer makes the surface hydrophobic and multilayer ice growth unlikely.[18] However, kaolinite is well known as a good nucleating agent. Both contrasting examples illustrate that lattice matching in heterogeneous ice nucleation can be an important factor but that it is not the only one. The influence of defects is also important, as revealed by experimental evidence of dramatic improvement of ice nucleation on pitted $BaF_2(111)$ surfaces

[a]Author to whom correspondence should be addressed. Electronic mail: averdaguer@cin2.cat.

through water immersion.[16] These results suggest that a $BaF_2(111)$ surface rich in defects is a better nucleation agent than a perfect $BaF_2(111)$ surface.

In this work we study water adsorption on freshly cleaved $BaF_2(111)$ surfaces in ambient conditions, that is at room temperature (RT) and variable relative humidity (RH), using different scanning force microscopy modes and optical microscopies and focusing on the role of atomic steps on the structure of the water films, which play a key role in the stabilization of water bilayers. An important outcome of this work is that steps running along different crystallographic directions show different wettabilities to the water bilayer, wettability confined to two dimensions defined by the step edges and terraces. The most hydrophilic steps correspond to $\langle \bar{1}10 \rangle$ directions, the main directions found on the surface after water immersion. We will show that a high density of kinks along steps does not forcibly guarantee higher wettability.

II. EXPERIMENTAL

All SPM experiments were carried out at RT with an Agilent 5500 atomic force microscope (AFM) (Agilent Technologies, Santa Clara, USA). The AFM was operated in the acoustic (*tapping*) mode and in a noncontact electrostatic mode called scanning polarization force microscopy (SPFM).[19] In this mode a conductive AFM tip is brought about 10–20 nm above the sample surface and electrically biased to a few volts with a modulated dc+ac voltage, creating attractive electrostatic forces between the tip and the polarizable surface. This mode allows a noncontact imaging of liquid films and droplets on surfaces simultaneously with contact potential measurements with nanometer resolution. The microscope head was enclosed in a glove box to control the environment. Humidity control was achieved by circulating dry N_2 to decrease RH or by bubbling N_2 through Milli-Q water to increase RH. RH was measured using a Digitron hygrometer. The RH uncertainly is $\pm 5\%$.

BaF_2 single crystals (Crystal GmbH, Berlin, Germany) were cleaved parallel to the (111) plane either at ambient conditions ($T=22\pm2$ °C, RH$\sim$50%) or inside the AFM globe box at low humidity ($T=22\pm2$ °C, RH$<$10%). Commercial Si tapping cantilevers (PPP-NCHR, Nanosensors, Neuchâtel, Switzerland), with resonance frequencies of $\sim$300 kHz and force constants of $\sim$50 Nm^{-1}, were used for acoustic mode and soft Pt coated cantilevers (PPP-CONTPt, Nanosensors) were used in the SPFM and contact experiments. Pt coated cantilevers had a nominal spring constant of $\sim$0.5 Nm^{-1}. SPFM experiments were performed at a frequency of 4 kHz, well below the cantilever resonance ($\sim$13 kHz).

Crystallographic directions on the surface of the crystals were determined by x-ray diffraction (Bruker D8 Advance, with a four-circle goniometer). The azimuth ϕ angles of the (200) reflections [threefold symmetry for the (111) BaF_2 oriented cut] were measured for each crystal. The projections of each [100] direction at the same ϕ angles on to the crystal surface correspond to $[2\bar{1}\bar{1}]$, $[\bar{1}2\bar{1}]$ and $[\bar{1}\bar{1}2]$ directions. Relevant $[11\bar{2}]$ and $[\bar{1}10]$ surface directions are readily derived from them.

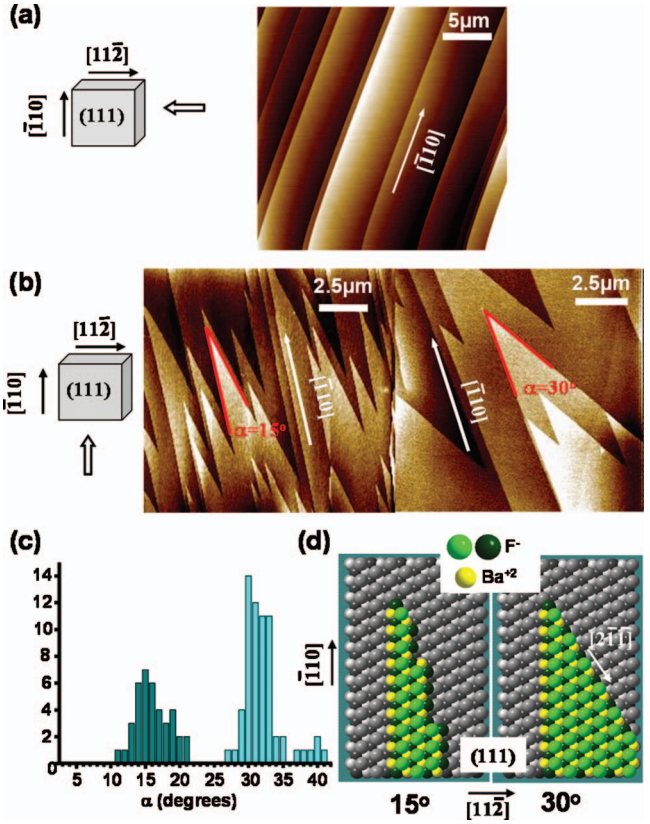

FIG. 1. [(a) and (b)] Topographic AFM images obtained in acoustic (*tapping*) mode of $BaF_2(111)$ surfaces obtained by cleavage along the $[11\bar{2}]$ and $[\bar{1}10]$ directions, respectively. All images were taken at 21 °C and RH$<$10%. Schemes showing the relevant directions, crystallographic and cleavage, are shown on top of the images. (c) Histogram of the distribution of angles between $[\bar{1}10]$ and other step directions for surfaces cleaved along the $[\bar{1}10]$ direction. (d) Representation of triangular steps on a $BaF_2(111)$ surface forming angle of 15° (left) and 30° (right), respectively. Fluorine and barium ions are represented by green and yellow balls, respectively, while the surface is represented by gray balls.

III. RESULTS

BaF_2 crystals were purchased in the form of (111)-oriented squared section parallelepipeds. The bars were cut in such a way that the exposed rectangular faces corresponded to orthogonal $\{\bar{1}10\}$ and $\{11\bar{2}\}$ family planes, respectively, as verified by x-ray diffraction. We arbitrarily assume that the relevant directions correspond to the $[\bar{1}10]$ and $[11\bar{2}]$ directions, respectively [see top of Figs. 1(a) and 1(b)], due to the cubic structure ($Fm\bar{3}m$ space group) of BaF_2. (111) surfaces were generated by cleavage using a blade. Stepped surfaces with micron-sized terraces were obtained as observed by AFM [see Figs. 1(a) and 1(b)]. The measured step heights were $\sim$0.4 nm, corresponding to the distance between adjacent trilayer planes (0.36 nm according to the known crystallographic structure). Higher steps were seldom observed, but always corresponding to integer multiples of 0.36 nm. It is important to note that different step shapes

were obtained depending on the direction of cleavage. Surfaces generated by cleavage along the $[11\bar{2}]$ direction exhibit most of the times terraces limited by parallel straight steps in the $[\bar{1}10]$ direction [Fig. 1(a)] while cleavage along the $[\bar{1}10]$ directions show lightning- or V-shaped steps [see Fig. 1(b)] as already reported on isostructural $CaF_2(111)$ surfaces.[20] Note that the direction of the tips of the triangular steps approximately corresponds to the direction of the crack propagation. Similar step distributions, parallel and V-shaped, have also been reported for (100) cleavage planes of monoclinic L-arginine phosphate monohydrate crystals, although their origin has not been discussed in detail.[21] One of the two main directions of the lightning-shaped steps corresponds to the $[\bar{1}10]$ direction [Fig. 1(b)] while the other direction is cleavage dependent. A histogram of the distribution of the acute angles (α) between both directions measured over many different samples is shown in Fig. 1(c). Two well differentiated groups of angles are observed, the most common one centered at $\alpha=30°$ and the other group centered in the 14°–19° range. Angles of 60°, 30°, and 19° have been reported on cleaved $CaF_2(111)$ surfaces, however, accurate measurements of angles on AFM images can be difficult due to drift during scanning which sometimes has lead to error in the analysis of the results.[22] Steps at 30° from the [-110] directions correspond to steps along the $[2\bar{1}\bar{1}]$ direction, as determined from the crystallographic structure [see Fig. 1(d) right]. Steps observed in the 14°–19° range do not run along well defined crystallographic directions suggesting that they consist of arrays of small $[\bar{1}10]$ and $[11\bar{2}]$ segments forming steps rich of kink sites [see Fig. 1(d) left].

Figure 2 shows topographic (left) and phase (right) AFM images taken in acoustic mode of water films grown on $BaF_2(111)$ at ambient conditions (T=21 °C and RH~45%). The difference in the tip-surface interaction when scanning over a *dry* terrace (no hint of adsorbed water) or over terraces partially covered with water induces a large contrast in the phase shift images (right side of the figure), making them ideal to visualize the water structures on the surface. In the phase images water appears in dark color representing larger interaction with the cantilever tip.[23] The relative small oscillation amplitudes chosen to minimize water-tip interaction prevents from changes in sign of the phase signal during scanning.[24]

The terraces are decorated with islands [see Fig. 2(a)], which exhibit an apparent height of ~0.5 nm that has been considered compatible with an ice I_h bilayer.[25] However, experimental evidences suggest that the solidlike structure of those water films differs from an I_h scenario.[14] Water films are also observed along straight steps, along $[\bar{1}10]$ directions as well as along the other step directions. In general water adsorbs preferentially at the lower terrace of the steps (lower trilayered atomic plane), although in some cases water accumulates on the higher terrace (the step belonging to this atomic plane). This can be clearly observed in Fig. 2(a). Appealing structures appear when the V-shaped steps are present at the surface [see, i.e., Fig. 2(b) and 2(c)]. Water becomes confined in the acute angles formed by steps of the same terrace. When water accumulates in the lower terrace

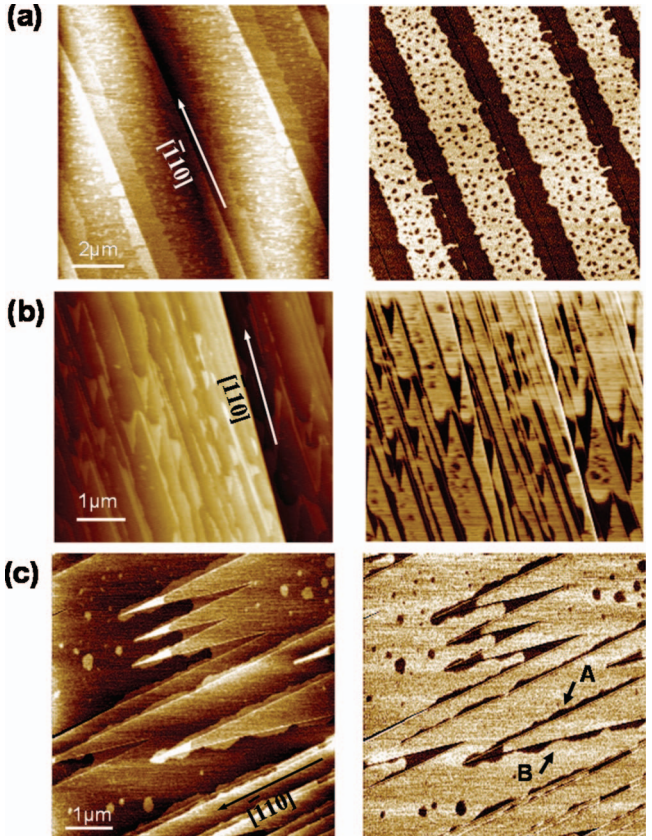

FIG. 2. Topographic (left) and phase (right) AFM images taken at ambient conditions (T=21 °C and RH~45%) in acoustic (tapping) mode of a $BaF_2(111)$ surfaces obtained by cleavage along: (a) the $[11\bar{2}]$ direction and (b) and (c) the $[\bar{1}10]$ direction]. In (c) steps running along $[\bar{1}10]$ and $[11\bar{2}]$ are indicated by A and B, respectively, highlighting different wettability behavior.

of the steps, it exhibits curved shapes resembling menisci wetting the steps. This is the 2D case of the 3D menisci formed between surfaces (think of water partially filling a glass cylinder). Examples can be also found in Fig. 3. Similar structures can be observed on the upper part of the tips of steps (upper terraces).

Accumulation of water on step edges may result from intrinsic surface diffusion of water molecules on the bare surface under ambient conditions and/or by tip-enhanced diffusion.[14] In order to address this important issue we show in Fig. 3(a) the time evolution of the water films while scanning over the same area. The comparison of the images, 1–3, readily evidences the perturbation induced by the tip. Note the formation of islands on the terraces, which were absent in the first image. Note also that some steps decorated in their lower terraces become undecorated and that the menisci become better defined after successive scans. Finally, we observe in the left side of the first image, roughly in its equator, a 2D droplet arising from a meniscus. The shape of this droplet changes until the droplet detaches and slips toward a close-lying step and the meniscus reservoir becomes emptied. A more evident example of how the tip can empty a reservoir is shown in the lower right part of the images (large meniscus in the central image). In order to ascertain the intrinsic or extrinsic nature of water confinement between steps we have taken images in the noncontact mode called SPFM

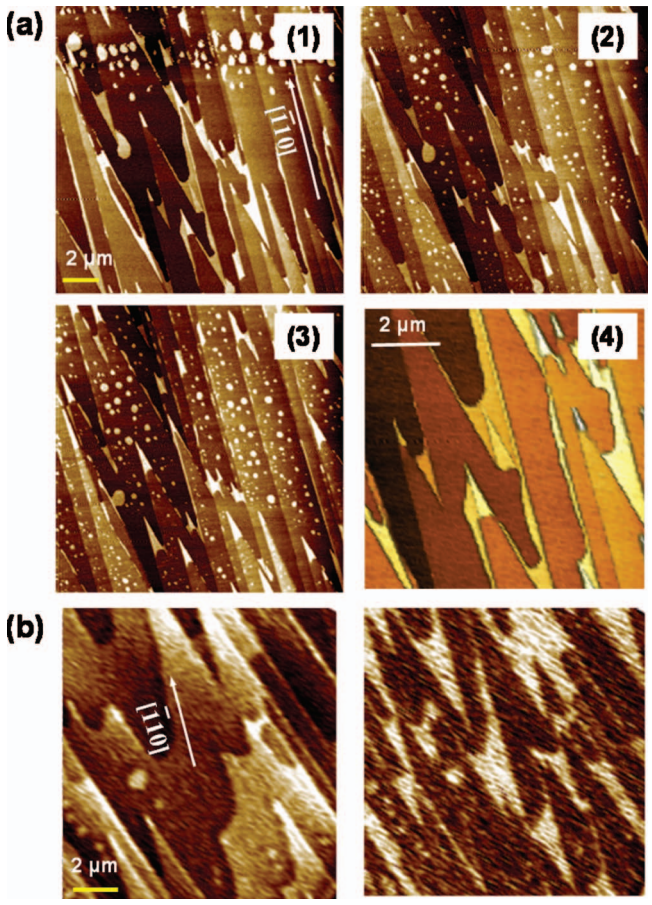

FIG. 3. (a) Topographic AFM images obtained in acoustic (tapping) mode of $BaF_2(111)$ surfaces obtained by cleavage along the $[\bar{1}10]$ directions. The images, (1)–(3), show the evolution after sequential scanning on the same region. The acquisition time per image is 170 s. Image (4) corresponds to a zoom of the central region of (1). The perturbation induced by the scanning tip can be observed in the formation of the different structures. (b) SPFM (left) and KPFM (right) images taken on a $BaF_2(111)$ surface. All images were taken at 22 °C and 50% RH.

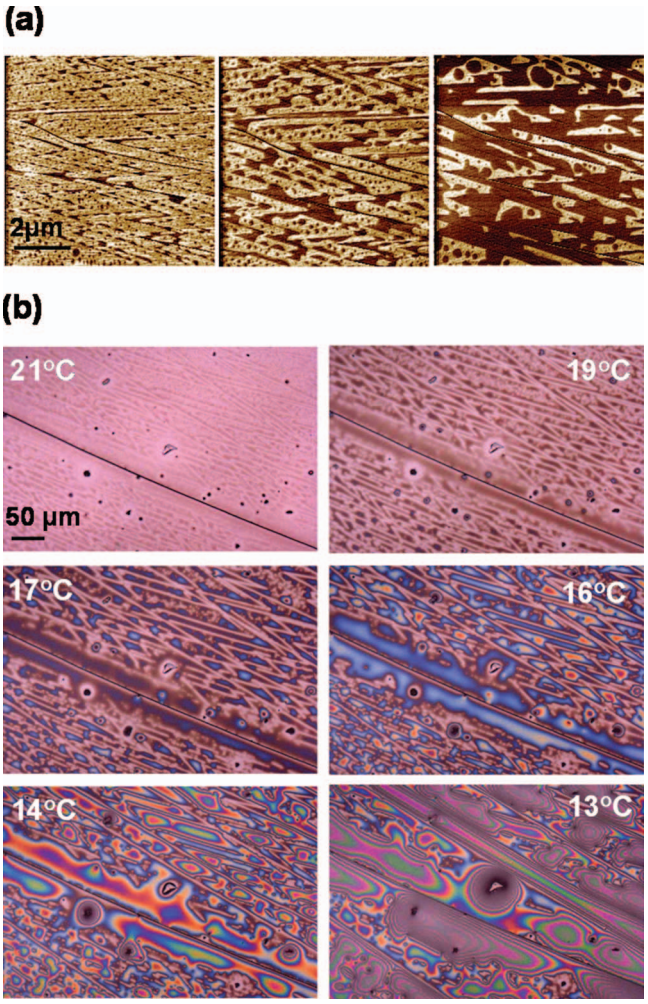

FIG. 4. (a) Phase AFM images of the evolution with increasing water coverage of water film structures on a highly stepped $BaF_2(111)$ surface. Images were taken at RT and RH ~ 50%. Increasing water coverage was induced by the AFM tip. (b) Optical microscopy images of a $BaF_2(111)$ surface obtained by cleavage along the $[\bar{1}10]$ direction. Images were taken at constant ambient RH ~ 55% and variable sample temperatures, indicated in the figure. As temperature decreases the relative humidity close to the surface increases and water adsorbs on the surface forming patterns very similar to the patterns formed by water bilayer patches observed using AFM.

used to obtain topographical and electrostatic properties of liquid films and droplets on surfaces.[19] The results are shown in Fig. 3(b). The left image shows the combined contribution from topography and dielectric response. In this case it is difficult to distinguish among step and water film edges because they show similar apparent heights. However, the Kelvin probe force microscopy (KPFM) image taken simultaneously (right image) shows a clear contrast between the water films (white color) and the dry $BaF_2(111)$ surface (dark color). The contrast between both regions (about +60 meV contact potential) in the KPFM images is induced by the averaged orientation of the water molecule dipoles pointing up from the surface at ambient conditions (21 °C, RH ~ 50%).[14] Since in SPFM the perturbation induced by the tip is negligible, the presence of menisci results from an intrinsic process (see discussion below). No significant difference in contrast was observed between water islands on the terraces and the water films at the triangular steps indicating that the dipole distribution on both films should be similar and suggesting a comparable bilayer structure in water films limited by steps and water films growing on terraces. In addition, the KPFM images show a homogeneous contact potential distribution over the water films again indicating a similar dipole orientation of the water molecules that are close to the steps and in the center of the film thus suggesting a similar structure within the lateral resolution of the images (~20 nm).

It is also remarkable that stable neighboring menisci sharing a common step exist [see Fig. 3(a)(4)], suggesting that flow of water molecules between both terraces is strongly reduced. This effect may be understood within the framework of the Ehrlich–Schwoebel model with efficient energy barriers at the step edges although no quantitative estimations of such barrier for this particular system are available.[26,27]

An alternative way of showing the intrinsic accumulation of water at steps is by using an optical microscope in an independent setup. In Fig. 4 a series of images of a freshly cleaved $BaF_2(111)$ surface taken at RH ~ 55% for decreasing sample temperatures is shown. Note that the steps are clearly

observed even at the moderate magnification used. Darker areas corresponding to the adsorbed water layers on $BaF_2(111)$ are observed to grow on the surface as the temperature of the sample is decreased (i.e., RH of the air close to the surface is increased). These dark areas show triangular structures very similar to what is observed by AFM. At some point water films are thick enough to show the well known interference pattern and overpass the step limitations inducing droplet coalescence. Although the observation of very thin water films with optical microscopy might be surprising,[28] just mention that recent examples of the observation of monoatomic graphene layers on SiO_2 have been reported.[29]

IV. DISCUSSION

Before initiating the discussion on the experimental results introduced in the previous section we would like to make a point on the experimental conditions. Our results have been obtained in ambient (real) conditions (RT and variable humidity) and, as a consequence, we are far from any ideal conditions (i.e., clean surfaces prepared in ultra high vacuum exposed to water doses).[30] Our approach implies two important issues: water vapor-film equilibrium and contamination. Contamination, mostly in the form of hydrocarbons, will be always present to some extent. However, experiments performed under ideal conditions are also not free from contamination as well established from x-ray photoelectron spectroscopy experiments, where the introduction of water vapor in surfaces prepared in UHV is always accompanied by hydrocarbons.[31] To conclude with contamination we confirm that our results are reproducible after measuring several freshly cleaved surfaces. Water vapor-film equilibrium will be discussed next.

A. Water-steps interactions

The accumulation of water at step edges, both on lower and higher lying terraces, as depicted from Figs. 2 and 3, is an evidence of the high diffusion of water on the $BaF_2(111)$ surface at RT. In a recent work, Shluger and co-workers[17] computed using density functional theory the diffusion barriers for water on $BaF_2(111)$ at RT to be 0.2 eV in the ideal case (water diffusing on defect free surfaces) and below 1 eV when different kinds of vacancies are considered, concluding that molecular water should be extremely mobile on this surface, as well as on the (111) surfaces of CaF_2 and SrF_2. These calculations are in line with our results, although they consider individual water molecules on both ideal and defective surfaces in a vacuum (no interaction with other water molecules) but in apparent contradiction with previous contact angle (θ) measurements[10] and with our own measurements, where the observed contact angles lie well below 15°, indicating almost perfect wetting.[32]

We thus have 2D structures, islands (most probably due to the nucleation of water around defects, i.e., fluorine vacancies, a nucleation that may imply water dissociation)[33] and water adhered to steps, in equilibrium with the water vapor pressure. At the RH achieved in the present work, the estimated coverage is below 1 ML, by direct comparison

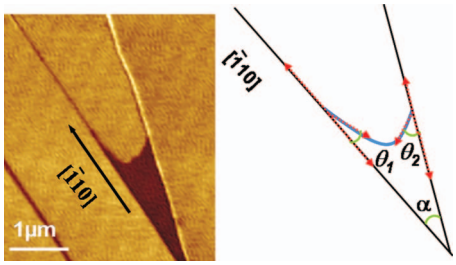

FIG. 5. (a) Phase AFM image obtained in acoustic (tapping) mode of a $BaF_2(111)$ surface obtained by cleavage along the $[\bar{1}10]$ direction. The image shows a detail of a water meniscus between two steps forming an angle of 15° evidencing two different contact angles. At the step along the $[\bar{1}10]$ crystallographic direction the contact angle is lower (more hydrophilic) than at the step at 15° from this direction. A scheme indicating the relevant angles and directions is shown in (b).

with isotherms of thin films of water on $BaF_2(111)$ at 25 °C as determined by Fourier transform infrared (FTIR) spectroscopy.[10] In this low coverage region it has been claimed that water is distributed as a 2D gas (absorption/desorption) and 2D bilayer structures, in agreement with our observations. According to the mentioned FTIR results, the highest adsorption enthalpy is found at ~0.75 ML with a value of ~0.58 eV in good agreement with the most stable bilayer structure (distorted and cross-linked chain) found by *ab initio* calculations (0.54 eV).[12] At lower coverages, ~0.2 ML corresponding to ~5% RH, the measured adsorption enthalpy is ~0.38 eV, which is very close to calculated binding energies of monomers of water on top Ba^{+2} ions from *ab initio* calculations (0.4 eV).[12,17] Such low energies suggest a scenario where water molecules readily diffuse as a 2D gas on the $BaF_2(111)$ surface.

Assuming equilibrium conditions, we can consider the 2D gas/2D bilayer system analog to water droplets in contact with a solid surface in equilibrium with water vapor but reduced to two dimensions. The wetting of the water films at the step edges will then be determined by the interplay of different interfaces, namely, vapor-substrate, vapor-water film, water film-substrate, vapor-step, water film edge-step, and vapor-water film edge. The steps should exhibit different interfacial energies or line tensions since they correspond to different crystallographic directions (see Fig. 1), so that we will label the corresponding line tension according to the angle that the step direction forms with respect to the $[\bar{1}10]$ direction: $\alpha=0°$ ($[\bar{1}10]$ itself), $\alpha=15°$, and $\alpha=30°$, respectively. The measured contact angles (θ) obtained from different images corresponding to different steps and different samples give $\theta=15\pm5°$, $\theta=50\pm10°$, and $35\pm5°$ for $\alpha=0°$, $\alpha=15°$, and $\alpha=30°$, respectively. Figure 5 shows the $\alpha=15°$ case. Note that water preferentially wets along the $[\bar{1}10]$ steps (more hydrophilic) and that the less hydrophilic step corresponds to $\alpha=15°$. This is at first sight surprising since one would expect a higher degree of water attachment for the direction corresponding to $\alpha=15°$, given the larger density of kinks relying on the ideal structure [Fig. 1(d)].

Defects at steps are known to play a key role as water nucleation sites. Hydroxide groups formed by water dissociation are known to be good nucleation sites, as discussed

above for terraces. In addition, the formation of BaO at step edges has been considered a better nucleation site for water than regular defect sites.[33] In our case, since our experiments provide no chemical information, we cannot be more explicit on this point. However, we do observe that the steps with presumably larger defect density turn out to be the less hydrophilic.

Contact angle values obtained along straight steps are not reliable due to pinning effects, thus information on wetting has to be extracted using a different approach. An example is shown in Fig. 2(c). The step running along the $[\bar{1}10]$ direction (A) is fully covered with water as it would be expected for a hydrophilic interface. However, the adjacent step (B) is covered with 2D droplets, thus exhibiting a less hydrophilic character. The additional modulation in shape is due to thermal fluctuations, where molecules flow along the steps (periphery diffusion), move from steps to terraces and then reattach to the step at different sites (terrace diffusion), and move between the steps and terraces with no correlation between motion at different sites (attachment-detachment).[34]

According to Marmur, θ does not depend on the geometry of the system (in this case triangular) if the motion of the contact line is not constrained.[35] In this case the measured contact angles correspond to their intrinsic values. The fact that for $[\bar{1}10]$ steps θ exhibits the same values for both the $\alpha=15°$ and $\alpha=30°$ geometries strongly suggests that the measured θ values correspond to intrinsic values, given that the defect density is higher for the $\alpha=15°$ case, which should induce a higher probability of pinning.

An analysis based on the heterogeneous growth model of Chernov,[36] where the Gibbs free energy of the system involving all interfaces is considered, does not lead to any quantitative conclusion since the concerned energies are unknown.[37] On the other hand one should be cautious when comparing calculated interfacial energies with experiments performed in ambient conditions since, to our knowledge, all such energies have been computed in ideal conditions, that is, involving solid-vacuum interfaces instead of solid-vapor interfaces.[38] In fact one would expect solid-vapor interfacial energies to be smaller than their solid-vacuum counterparts, based on experimental evidences.[39] We believe that the involved interfacial energies should be of the order of 0.073 Nm^{-1}, the well-known value for vapor-liquid interfaces for pure water and at RT (surface tension), and well below the surface energy value of the (111) surface of BaF_2, estimated to be 0.33 Nm^{-1} according to *ab initio* calculations.[40] As an illustrating example, just mention the case of the liquid water-ice interfacial energy, which has been experimentally determined as 0.03 Nm^{-1}.[41] We should add that the reduction of the water bilayers down to nanometric dimensions should increase the interfacial energies, as suggested by experimental evidence by grazing-incidence x-ray scattering[42] and AFM[23] measurements.

The apparent contradiction of a weak water-surface interaction, as theoretically predicted and experimentally verified, which leads to a high surface diffusion and the observed macroscopic high degree of wettability, can be thus explained by the accumulation of water at steps, where those along the $[\bar{1}10]$ directions significantly contribute due to their hydrophilic character.

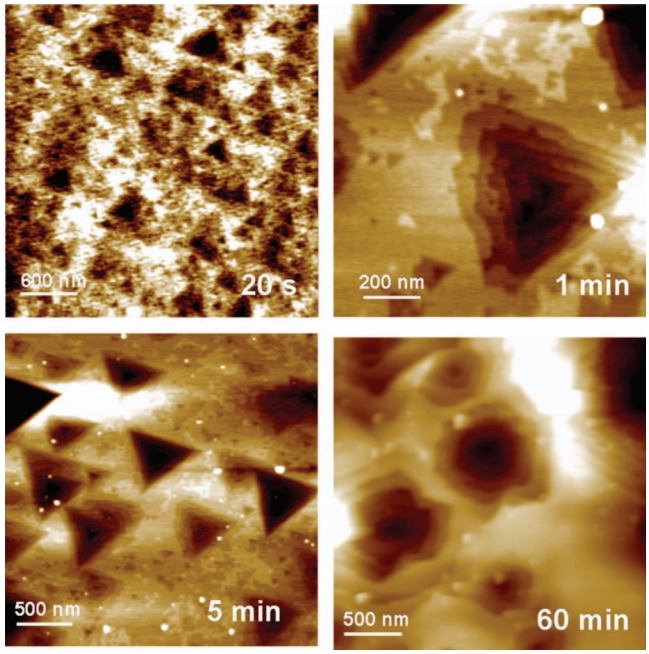

FIG. 6. Topographic AFM images obtained in acoustic (tapping) mode of $BaF_2(111)$ surfaces obtained by cleavage and then immersed in water for different times: 20 s, 1 min, 5 min, and 60 min. For immersion times higher than 15 s triangular pits produced by water etching can be observed. The directions of the triangles correspond to $\langle\bar{1}10\rangle$ crystallographic directions. For large immersion times triangular as well as hexagonal step structures can be observed. All images were taken at RT and low humidity conditions (RH $<$ 10%).

B. Water-induced surface pitting

As mentioned above, Conrad *et al.* showed experimentally that the pitting of a submerged $BaF_2(111)$ surface dramatically improves its ice nucleating ability.[16] In that study AFM images of $BaF_2(111)$ surfaces are shown after immersion in water. The topography evidences rough surfaces with pit patterns with heights of 20–40 nm. We decided to do a more complete examination of the modifications of the $BaF_2(111)$ surface induced by water dissolution. Freshly cleaved $BaF_2(111)$ crystals were immersed in Milli-Q water for a controlled amount of time and then dried with nitrogen and immediately imaged with AFM. In Fig. 6 we show images of the surface for different immersion times. For short times a homogeneous roughness of the surface is observed and the triangular structures start to become visible. For immersion times larger than 15 s, triangular etching pits can be clearly observed on the surface. A close look at the pits reveals a stepped structure that forms equilateral triangles over the entire surface. The directions of the steps forming those triangles correspond to $\langle\bar{1}10\rangle$ directions, which are hydrophilic as discussed above. For larger times structures with steps forming angles of 60° and 120° can be observed on the surface, again all of them belonging to the $\langle\bar{1}10\rangle$ family. Such structures are very similar to those formed by etching of different substances on $CaF_2(111)$.[43] A surface rich on

such steps would induce a network of water bilayers stabilized by the steps and would enhance multilayer ice growing in a more efficient way as compared to cleaved $BaF_2(111)$ surfaces.

V. CONCLUSIONS

We have studied the role of steps in the interaction of water with freshly cleaved (111) surfaces of BaF_2 single crystals in ambient conditions using different SFM imaging methods and optical microscopy. We have shown the stabilizing effect of steps for the growth of the two-dimensional water patches. Such water patches are preferentially observed on terraces limited by triangular steps created by cleavage. These patches are larger for lower terraces and show a meniscuslike shape that can be related to the different wettability of the steps. We found that steps running along the $[\bar{1}10]$ directions are by far the most hydrophilic steps beating even steps with high density of kinks. Our results prove that morphological defects such as steps can be crucial for improving monolayer wetting and stabilization of multilayer grown on surfaces that show a good lattice mismatch relationship with water molecules forming ice.

We believe that a theoretical study of the interaction of water molecules with stepped surfaces would be of great interest in order to clarify the underlying mechanism of water absorption. A realistic situation would need to involve a large number of water molecules per substrate unit cell since the individual molecule scenario may not be representative of a real (ambient conditions) situation.

ACKNOWLEDGMENTS

We thank Dr. E. Artacho and Dr. P. Ordejón for illuminating discussions and J. J. Segura and A. Monistrol for helping in the preparation of the experimental setup. This work was supported by the Ministerio de Educación y Ciencia (MEC), Spain, through Project No. FIS2006-12117-C04-01 and by Generalitat de Catalunya (SGR 00909). A.V. acknowledges support from the Spanish Ramón y Cajal Program (MCINN).

[1] B. J. Mason, *The Physics of Clouds* (Clarendon, Oxford, 1971).
[2] I. Langmuir, Science **112**, 35 (1950).
[3] W. Cantrell and A. Heymsfield, Bull. Am. Meteorol. Soc. **86**, 795 (2005).
[4] A. Verdaguer, G. M. Sacha, H. Bluhm, and M. Salmeron, Chem. Rev. (Washington, D.C.) **106**, 1478 (2006) and references therein.
[5] B. Vonnegut, J. Appl. Phys. **18**, 593 (1947).
[6] National Research Council, *Critical Issues in Weather Modification Research* (National Academics Press, Washington, D.C., 2003).
[7] P. A. Thiel and T. E. Madey, Surf. Sci. Rep. **7**, 211 (1987) and references therein.
[8] J. J. Segura, A. Verdaguer, M. Cobián, E. R. Hernández, and J. Fraxedas, J. Am. Chem. Soc. **131**, 17853 (2009).
[9] J. E. Zink, J. Reif, and E. Matthias, Phys. Rev. Lett. **68**, 3595 (1992).
[10] V. Sadtchenko, P. Conrad, and G. E. Ewing, J. Chem. Phys. **116**, 4293 (2002).
[11] V. Sadtchenko, G. E. Ewing, D. R. Nutt, and A. J. Stone, Langmuir **18**, 4632 (2002).
[12] D. R. Nutt and A. J. Stone, J. Chem. Phys. **117**, 800 (2002).
[13] J. Vogt, J. Chem. Phys. **126**, 244710 (2007).
[14] A. Verdaguer, M. Cardellach, and J. Fraxedas, J. Chem. Phys. **129**, 174705 (2008).
[15] G. E. Ewing, Chem. Rev. (Washington, D.C.) **106**, 1511 (2006).
[16] P. Conrad, G. E. Ewing, R. L. Karlnsey, and V. Sadtchenko, J. Chem. Phys. **122**, 064709 (2005).
[17] A. S. Foster, T. Trevethan, and A. L. Shluger, Phys. Rev. B **80**, 115421 (2009).
[18] X. L. Hu and A. Michaelides, Surf. Sci. **602**, 960 (2008).
[19] J. Hu, X.-D. Xiao, and M. Salmeron, Appl. Phys. Lett. **67**, 476 (1995).
[20] J. Engelhardt, H. Dabringhaus, and K. Wandelt, Surf. Sci. **448**, 187 (2000).
[21] Y. L. Geng, D. Xu, X. Q. Wang, G. W. Yu, G. H. Zhang, and H. B. Zhang, J. Cryst. Growth **282**, 208 (2005).
[22] J. Engelhardt, H. Dabringhaus, and K. Wandelt, Surf. Sci. **516**, 216 (2002).
[23] J. Fraxedas, A. Verdaguer, F. Sanz, S. Baudron, and P. Batail, Surf. Sci. **588**, 41 (2005).
[24] R. García and A. San Paulo, Phys. Rev. B **60**, 4961 (1999).
[25] K. Miura, T. Yamada, M. Ishikawa, and S. Okita, Appl. Surf. Sci. **140**, 415 (1999).
[26] G. Ehrlich and F. G. Hudda, J. Chem. Phys. **44**, 1039 (1966).
[27] R. L. Schwoebel and E. J. Shipsey, J. Appl. Phys. **37**, 3682 (1966).
[28] We have applied the Fresnel equations in order to calculate the contrast induced by a water film on $BaF_2(111)$ for different wavelengths. Contrast is defined as the relative intensity of reflected light in the presence and absence of a water film. Maximum contrast is obtained for violet and blue wavelengths. At a wavelength of 410 nm we obtain the following contrasts for different water thicknesses: (1nm, 0.03%), (5 nm, 0.8%), (10 nm, 3%), and (20 nm, 12%); H. Anders, *Thin Films in Optics* (Focal, London, 1967).
[29] P. Blake, E. W. Hill, A. H. Castro Neto, K. S. Novoselov, D. Jiang, R. Yang, T. J. Booth, and A. K. Geim, Appl. Phys. Lett. **91**, 063124 (2007).
[30] A. Lehmann, G. Fahsold, G. König, and K. H. Rieder, Surf. Sci. **369**, 289 (1996).
[31] A. Verdaguer, Ch. Weiss, G. Oncins, G. Ketteler, H. Bluhm, and M. Salmeron, Langmuir **23**, 9699 (2007).
[32] Contact angle measurements performed in a KRUSS EasyDrop Standard system using BaF_2 single crystals from the same batch and cleaved in the same way, give values below 15° and in many case below the instrument experimental limit (~6°).
[33] Y. Wu, J. T. Mayer, E. Garfunkel, and T. E. Madey, Langmuir **10**, 1482 (1994).
[34] H.-C. Jeong and E. D. Williams, Surf. Sci. Rep. **34**, 171 (1999).
[35] A. Marmur, Langmuir **12**, 5704 (1996).
[36] A. A. Chernov, *Modern Crystallography III: Crystal Growth* (Springer, Berlin, 1984).
[37] Low adhesion is modeled by $\Delta\gamma>0$, where $\Delta\gamma=\gamma_{vw}+\gamma_{ws}-\gamma_{vs}$ and γ_{vw}, γ_{ws} and γ_{vs} represent the vapor-water film (vw), water film-substrate (ws), and vapor-substrate (vs) interfacial energies, respectively, which are defined as positive. The maximization of the Gibbs free energy of formation of the water films leads to the condition $\Delta\mu>0$, where $\Delta\mu$ stands for the chemical potential per unit volume, since $\Delta\gamma>0$, see, i.e., J. Fraxedas, *Molecular Organic Materials* (Cambridge University Press, New York, 2006), pp. 208–212. Both conditions, $\Delta\mu>0$ and $\Delta\gamma>0$, indicate that the films grow according to the Volmer–Weber mechanism (incomplete wetting) (Ref. 36).
[38] V. E. Puchin, A. V. Puchina, M. Husinga, and M. Reichling, J. Phys.: Condens. Matter **13**, 2081 (2001).
[39] A. I. Bailey and S. M. Kay, Proc. R. Soc. London, Ser. A **301**, 47 (1967).
[40] H. Shi, R. I. Eglitis, and G. Borstel, J. Phys.: Condens. Matter **18**, 8367 (2006).
[41] S.-N. Luo, A. Strachan, and D. C. Swift, Modell. Simul. Mater. Sci. Eng. **13**, 321 (2005).
[42] C. Fradin, A. Braslau, D. Luzet, D. Smilgies, M. Alba, N. Boudet, K. Mecke, and J. Daillant, Nature (London) **403**, 871 (2000).
[43] Ch. Motzer and M. Reichling, J. Appl. Phys. **105**, 064309 (2009).